Performance Enhancement of a Morphing Limb for an Amphibious Robotic Turtle

Jiefeng Sun, Brandon Lin, Luis A. Ramirez, Esteban Figueroa,
Robert Baines, Bilige Yang, Erick Marroquin, and Rebecca Kramer-Bottiglio

Abstract— Terrestrial and aquatic animals exhibit appendages adapted to the propulsion physics of their primary habitats. Terrestrial appendages typically assume stiff and load-bearing form factors, while aquatic appendages tend to adopt flexible and streamlined profiles. Bio-inspired robots with synthetic appendages often mirror this dichotomy of specialization: they are designed with fixed legs or flippers for locomotion on land or in water, respectively. Appendages that adjust their shape and stiffness can serve to specialize a robot's propulsion physics on demand, enabling transitions between multiple environments. Herein, we report a morphing limb combining layer jamming and pouch-based pneumatic actuation that rapidly and efficiently switches between a flexible flipper for swimming and a rigid leg for walking/crawling. The internal pouch actuator contributes to pressure that jams the external layers of the limb, which we refer to as positive pressure-reinforced jamming. We quantify the extent of shape-morphing conferred by the pouch actuator, the maximum load-bearing capability of the limb in leg mode, and the hydrodynamic characteristics of the limb in flipper mode. We find that the new limb boasts better performance than previous designs with respect to morphing shape, speed, efficiency, and hydrodynamics. Crucially, we also find that positive pressure-reinforced jamming increases the leg's compressive strength by 30% relative to just jamming the layers via negative pressure. With its own lightweight and compact electronics system, the morphing limb is a plug-and-play component for building an untethered multi-environment robot.
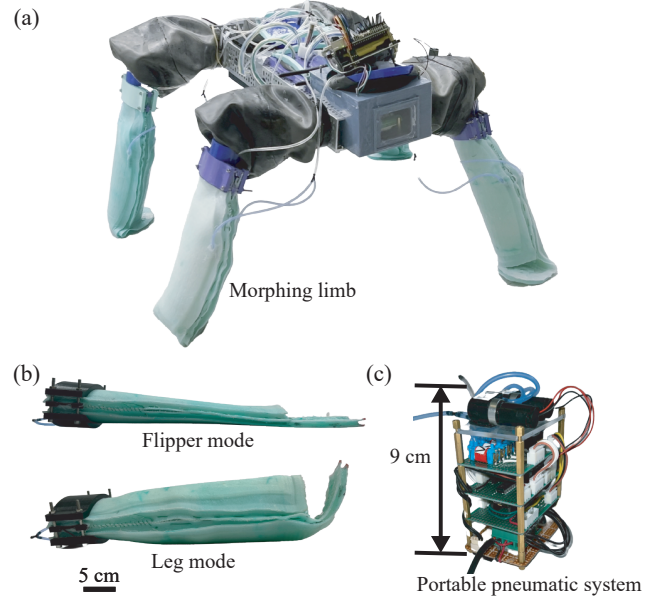
Fig. 1. (a) An amphibious robotic turtle with a morphing limb for multi-environment locomotion. (b). The morphing limb can transition between a flipper shape and a leg shape. (c) A portable pneumatic system facilitates tether-less operation of the limb's morphing process.

I. INTRODUCTION

Adapting robot limb morphology has proven to be a viable strategy to navigate diverse terrains and transition between different physical environments (*i.e.*, water vs. land) [1], [2]. The optimization of morphing limbs is a complex challenge, due to the different shapes and stiffnesses required for effective locomotion in different environments [3]. For example, in water, limbs should ideally function as hydrodynamic surfaces, sustaining distributed forces while accommodating pressure gradients created by propulsive movements [4], [5]. On land, limbs should support the robot's weight while exhibiting spring-like behavior for agile movement [6].

Many strategies have been explored to manipulate the stiffness and geometry of robotic limbs [7], [8]. For example, researchers developed robots with limbs capable of melting and solidifying thermoplastic joints, allowing them to adapt

their movement kinematics on demand [9]; adjusting their leg lengths using linear actuators to optimize their cost of transport on different surfaces [10]; adapting their structural configuration from wheel-like to flipper-like for amphibious propulsion [11]; and changing their inflation state to improve traction on land or increase propulsion in water [12].

Prior work demonstrated a robotic limb that transitions from a flipper shape (for aquatic swimming) to a load-bearing leg shape (for land walking or crawling) via a thermally-responsive variable stiffness epoxy adhered to pneumatic bending actuators [13]. Neutrally in the flipper shape, the epoxy could be warmed above its glass transition temperature to soften it for morphing. The pneumatic bending actuators could then morph the limb into its leg shape, and the epoxy was cooled to hold the new shape passively. Warming the limb would again soften the epoxy and return the limb to its flipper shape. Realizing these morphing limbs in a quadruped robot yielded sea turtle- and land tortoise-inspired multi-environment robotic transitions [1].

The version of the morphing limb presented in [13] and [1] included a thermally-responsive material, which coupled its energetic cost of morphing to the environmental temperature. A more recent (though unpublished at the time of

Version	Weight	Morphing Energy	Actuation Pressure	Flipper Thickness	Max Load (Vertical)	Glide Ratio
V1: Epoxy [1]	350 g	10360 J	30 psi	16 mm	600 N	1.4
V2: Jamming	450 g	146.5 J	30 psi	30 mm	450 N	1.1
V3: This work	260 g	95 J	2 psi	10 mm	220 N	2

TABLE I

COMPARISON OF PERFORMANCE METRICS BETWEEN ITERATIONS OF MORPHING LIMBS FOR THE AMPHIBIOUS ROBOTIC TURTLE.

this writing) version of the limb uses topologically altered "kirigami" laminar jamming [14] to morph between the hydrodynamic flipper and load-bearing leg shapes. With a pressure-responsive layer jamming system for variable stiffness, the jamming limb decouples its morphing performance from the environmental temperature and further achieves rapid stiffness adjustments.

However, the kirigami layer jamming limb design faced two critical issues. First, generating sufficient geometric changes through the pneumatic bending actuators proved arduous. Morphing from flipper to leg shapes required pressures exceeding 30 psi, which made it difficult to untether the robot. Second, the switch from epoxy to layer jamming as a variable stiffness material increased the limb's thickness, improving load-bearing, but sacrificing hydrodynamics.

In this study, we introduce a refined morphing limb design that captures the advantages of both the epoxy limb's hydrodynamic profile and the jamming limb's approach to rapid, environment-agnostic stiffness switching (Fig. 1a,b). The limb retains laminar jamming for variable stiffness but uses a new fluidic actuation strategy. We replaced the prior external fluidic actuators with a single pouch actuator, which couples the inflation that drives the flipper-to-leg cross-section shape change with the curvature of the limb's tip (the "foot"), thus reducing the total actuator count from three to one per limb. Since the limb's compressive modulus increases with both decreasing pressure in the layer jamming components and increasing pressure in the pouch actuator, we call this design "positive pressure-reinforced jamming."

The stiffness contribution from the pouch actuator allows for a substantial reduction in the number of layers within the laminar jamming components. Hydrodynamic characterizations suggest that the new limb's flipper profile is improved relative to prior versions, both when jammed (stiff) and unjammed (soft). Utilizing onboard 2.5 W pumps (Fig. 1c), the limb executes morphing sequences within 38 s, consuming 95 J of energy. A comparative analysis of the limb against prior designs is shown in Table I. We note that tethered pumps drive the prior designs, denoted as V1 and V2 in Table I, due to high-pressure requirements and that these pumps consume relatively more energy.

II. MORPHING LIMB DESIGN

As shown in Fig. 2, for morphing into and maintaining flipper and leg shapes, the limb combines kirigami layer jamming [14] with an internal pouch actuator. The internal pouch deforms the layers and induces a bend in the limb's tip through a cable mechanism, while layer jamming functions as a variable stiffness component that softens for morphing and stiffens to hold a target shape.

A. Pouch actuator

The pouch actuator is a pneumatic artificial muscle constructed from a thin, inextensible, yet highly flexible film that is heat-formed into a pouch. Typically, pouch actuators generate linear contraction with little radial expansion. Our approach leverages radial expansion and contraction in tandem to alter the limb's cross-sectional shape (and consequently, its bending stiffness) as well as the curvature of the tip, respectively. Moreover, the pouch's expansion reinforces the strength of the layer jamming components, akin to the principles of positive pressure jamming [15].

Fig. 3. (a) The fabrication process of the pouch actuator. 1: Fold a sheet of air-tight film in half. 2: Seal the folded sheet at the designated width. 3: Create internal folds along the sides of the sheet. 4: Create seals at the top and bottom of the pouch. A thin PET sheet is inserted at the top to create an opening for the pneumatic tubing. 5: Insert the pneumatic tubing and seal it within the pouch using hot glue. 6: Seal a thin strip of air-tight film to the top of the pouch to create a hood for anchoring the pouch within the circular housing. (b) The pouch actuator before and after inflation.

Initial trials employing a conventional pouch actuator with no folding [16] revealed inadequate contractile displacement
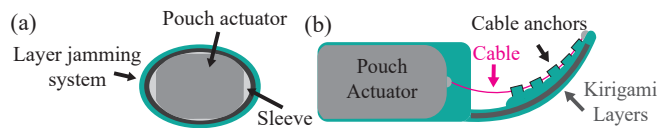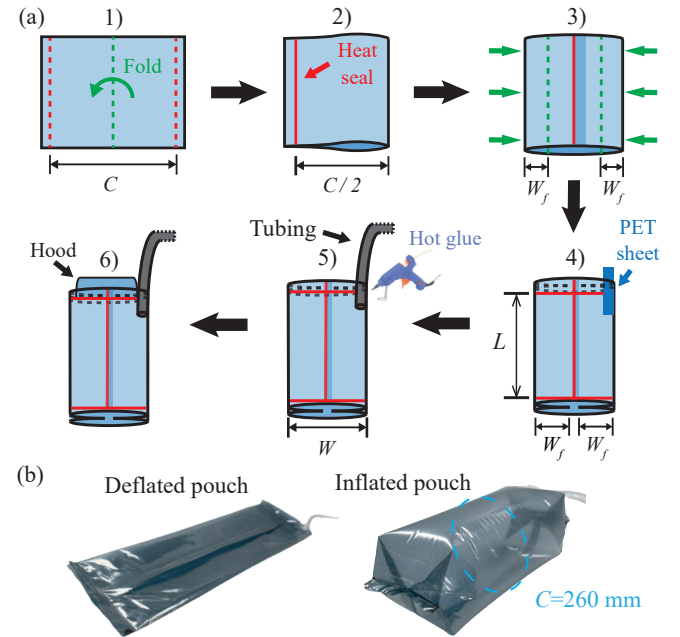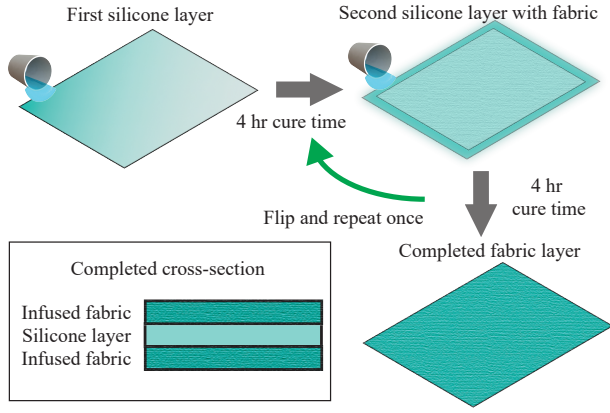

Fig. 2. The working principle of the shape morphing limb. (a) The limb cross-section. (b) The cable mechanism bends the tip during actuator contraction.

Fig. 4. Fabrication of the silicone-infused double-layer fabric (SIDF).

Fig. 5. The fabrication process of the layer jamming system part A and B, with the integration of the topologically augmented (kirigami) layers.

at maximum expansion. To address this limitation, we created pouches with folds to generate the necessary contractile displacement to achieve tip bending [17]. Fig. 3 illustrates the fabrication steps for the folded pouches. For the pouch material, we opted for heat-sealable film (amine-free polyethylene from McMaster-Carr, 4663T9), as heat sealing simplifies the manufacturing process. Alternative materials such as heat-sealable nylon fabrics and silicone-infused fabric could be considered to enhance the pouch's strength and durability.

We denote the pouch's initial circumference (unfolded width) as C, the side-fold widths as W_f, the pouch length as L, and the final pouch width as W. The folding ratio W_f/W is correlated to the contraction generated when the pouch's length, L, is held constant [17]. Based on our experimental findings, a folding ratio exceeding 0.5 results in folding overlaps and increases the risk of pouch leakage due to the additional layers that must be heat-sealed. Therefore, we opted for a folding ratio of 0.5, resulting in $C = 4W = 8W_f$. This ratio achieved the desired tip bending, as demonstrated in Section III-A.

B. Layer jamming system

The layer jamming system comprises silicone-infused double-layer fabric (SIDF) serving as an airtight envelope in which cut polyethylene terephthalate (PET; 0.01 in thick) sheets are positioned. The SIDF is composed of two layers of silicone-impregnated fabric enveloping a central layer of silicone. The outer layer of fabric is resilient to external penetration, particularly when the limb encounters rough terrain, while the inner layer serves to protect against abrasion from the PET sheets contained inside.

The fabrication of SIDF involves three steps, depicted in Fig. 4. Initially, an airtight layer of silicone (EcoFlex-50, Smooth-on Inc.) is cast onto a smooth surface. After curing, additional silicone is evenly applied atop the airtight layer, and a layer of fabric (poly-cotton and polyester) is immediately placed on it and flattened via scraping motions with a ruler to ensure a secure interfacial bond. This process also facilitates complete silicone infusion into the fabric. Subsequently, the assembly is flipped over, and another layer of fabric is bonded in the same manner.
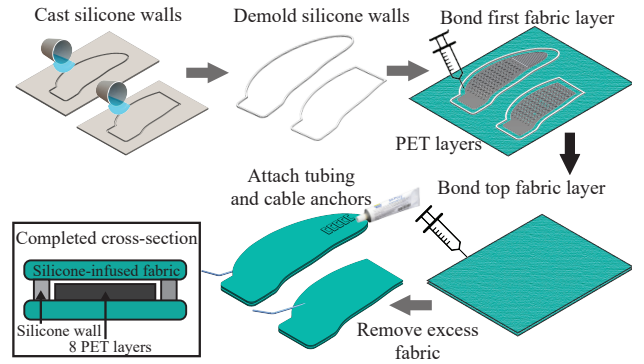
The complete fabrication procedure for the kirigami layer jamming system is shown in Fig. 5. First, a silicone wall conforming to the limb's shape is cast. Subsequently, this silicone wall is affixed to the SIDF housing eight layers of PET sheets. These PET sheets are laser-cut into the desired limb shapes, denoted as A and B. The choice of limb shape is detailed in [13]. To optimize the jammed-to-unjammed flexural stiffness ratio, we selectively removed material from the sheets to augment the second moments of area of the jammed and unjammed states, following guidelines proposed in [14]. A silicone tube is threaded through a hole in the envelope surrounding the jamming sheet and sealed with adhesive (Silpoxy, Smooth-on Inc.).

C. Morphing limb assembly

Fig. 6a shows an exploded view of the morphing limb. We first sew parts A and B of the jamming system together along their edge, as shown in Figure 6b. We then insert the pouch between the two jamming walls, using a sleeve to reduce the friction. An assembly comprising two clamps a circular housing, and a carbon fiber rod serves to anchor the pouch actuator and interface to the shoulder joints of our amphibious robot body. A cable (fishing line) is fixed between the pouch and the limb's tip, to pull the tip inward when the pouch contracts.

D. Electrical system

We designed a compact and portable electrical system to facilitate the untethered mobility of future amphibious robots equipped with the limb. The electrical system consists of two micro diaphragm pumps (Dynaflo, 2000 series), four valves (V1-V4; Park, X-Valves, 30 psi, normally closed), and two pressure sensors (S1, S2; 015PGAA5, 030PGAA5; Honeywell). An Arduino Nano is used as an onboard microcontroller, sending signals to the motor driver (TB6612FNG) and the transistor array (TBD62083APG-ND), which respectively drive the two pumps and the four valves and sample the pressure data.

As illustrated in Fig. 7a, the system employs two pumps: P1 is responsible for inflating the pouch actuator, while P2 manages the vacuuming of the jamming system. Given
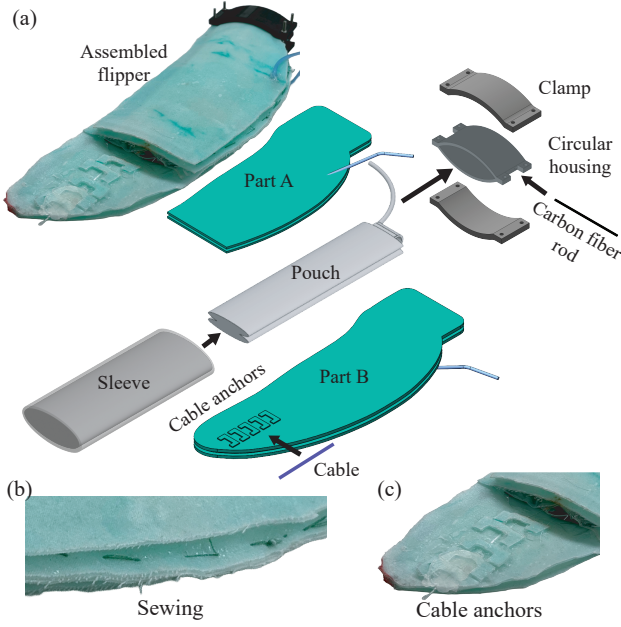
Fig. 6. (a) The fully assembled limb, displayed with an exploded view. (b) The sewing method to attach Parts A and B of the layer jamming system. (c) Cable anchors constrain the cable that pulls the tip of the limb inwards.

Fig. 7. (a) A schematic of the pneumatics system. (b) The truth table of the pneumatic control logic.

the limb's intended application for an amphibious robot, it necessitates enclosure within a waterproof housing to ensure protection (labeled as "Container" in Fig. 7a). Additionally, the exposed tubing incorporates an actively controlled valve (V1), serving as a safeguard against water ingress during underwater operations. The pneumatic pressure sensors play an integral role by continuously measuring the pressure within both the pouch and the jamming system, enabling closed-loop control of the pumps. For reference, Fig. 7b provides the truth table for the pneumatic valves during the morphing sequence, where "1" indicates that the valves or pumps are active, and "0" signifies that they are deactivated.

III. MORPHING LIMB CHARACTERIZATION

A. Limb shape actuation

When the internal pouch actuator inflates, the limb's cross-section transforms from flat to oval. To characterize the relationship between the pouch pressure (P_p) and the limb's diameter expansion (d), we conducted experiments shown in Fig. 8. We placed a marker atop the flipper to visually track the expansion while slowly inflating the pouch (Fig. 8a). Using a recording and subsequent tracking software (Tracker; physlets.org/tracker), we analyzed the changes in d as a function of P_p. The coupled bending angle of the limb's tip was also tracked. Three color markers were distributed on the edge of the tip. Since the three dots are almost on a straight line, the bending angle was calculated as the angle between a vector through the two tracking dots (close to the tip) and the horizontal line.

Because the layer jamming system that constrains the pouch has varying widths (Fig. 8b), different pouch circumferences were tested to optimize the expansion: 180, 220,
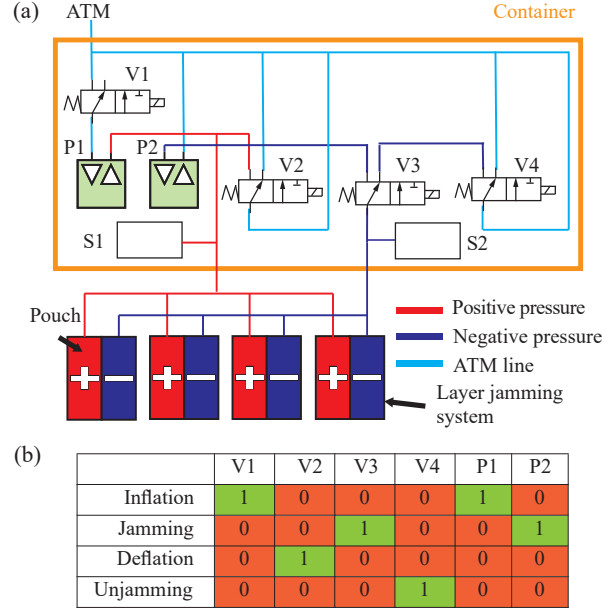
260, and 300 (all mm). As shown in Fig. 8d, the diametric expansion increases with increasing pressure for all pouch sizes tested, and plateaus after 1.5 psi. The pouch with the largest expansion is $C = 260$ mm, which is slightly larger than the maximum designed circumference of the layer jamming system (220 mm in Fig. 8b). We suspect that the layer jamming system plastically deforms due to pouch actuation to accommodate the pouch's 260 mm circumference, but not so much to accommodate even larger pouches.

Fig. 8e shows that the tip bends by more than $70°$ after the pouch inflates to 2 psi, which prevents it from uncurling while the robot is walking. We also observed that the tip bending angle increases when the layer jamming system is engaged ($P_j = -13$ psi), because the clearance between the SIDF and PET layers reduces (Fig. 8c).

Fig. 8f depicts the expansion and bending angle when $P_p = 2$ psi and $P_j = -13$ psi. The maximum bending angle occurs with $C = 220$ mm; the largest expansion is with $C = 260$ mm. We surmise that $C = 260$ mm did not have the largest tip bending due to the physical constraints imposed by the layer jamming system. We chose $C = 260$ mm for subsequent characterizations, since it achieves the largest expansion and has a tip bending angle larger than $60°$ (the minimum required to prevent uncurling).

B. Compression testing in leg mode

During terrestrial gaits, the morphing limb (in leg mode) needs to withstand compression loads from various angles. To determine the limb's load-bearing capability, an Instron 3345 equipped with a 1 kN load cell was used to measure force-displacement curves for the limb in vertical and horizontal orientations corresponding to waking and crawling.

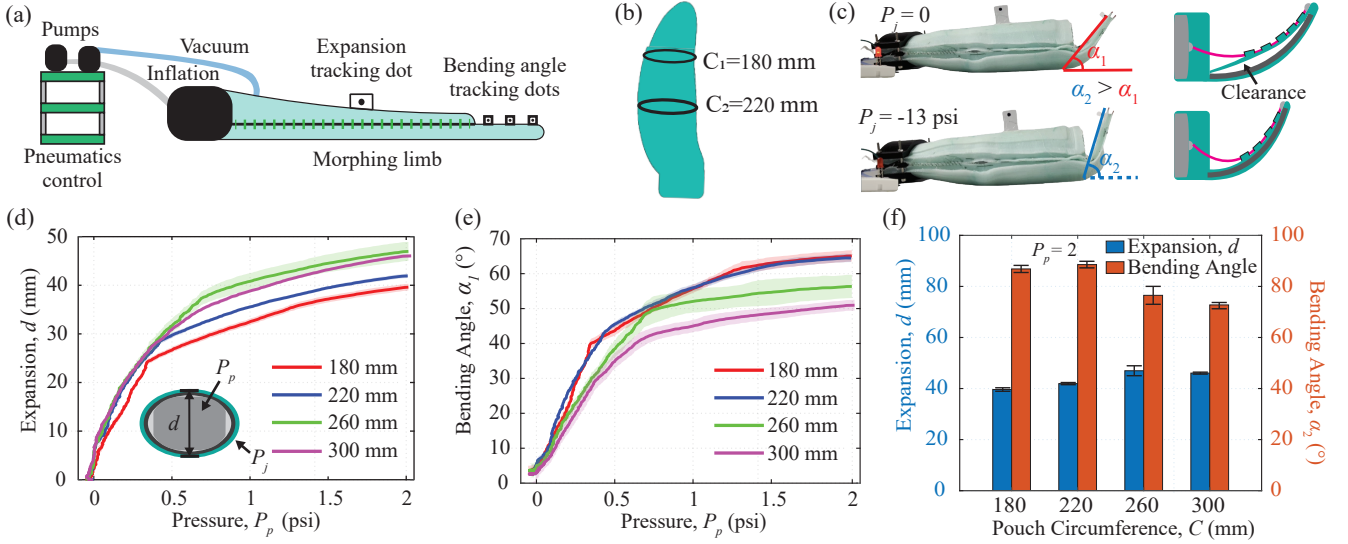We tested five limb conditions in the vertical orientation,

Fig. 8. (a) The setup for the pouch actuation tests. (b) The inner circumference of the layer jamming system varies between 180 and 220 mm. (c) Bending angle increases following the jamming of the limb. Images of the limb before jamming display a large amount of slack between the cable and the fabric; this slack is removed upon jamming. (d) Limb expansion vs. pouch pressure before jamming. (e) Limb tip bending angle vs. pouch pressure before jamming. (f) The maximum values for limb expansion and tip bending angle after jamming.

listed in Fig. 9a: **1)** unjammed flipper (pouch deflated, jamming off), **2)** jammed flipper (pouch deflated, jamming on), **3)** jammed leg (pouch initially inflates, then jamming holds shape with pouch deflated), **4)** unjammed leg (pouch inflated, jamming off), and **5)** positive pressure-reinforced jammed leg (pouch inflated, jamming on). The positive pressure-reinforced jammed leg shows a 30% increase in maximum load-bearing capability (peak force) when compared with the jammed leg or unjammed leg. Assuming the robot has its weight (18.5 kg) equally distributed between its four limbs, the maximum load that a limb needs to withstand is 20 N. The results suggest that all limb conditions would sufficiently support the robot, except the flipper conditions.

Fig. 9b shows a loading condition representative of a crawling gait. The results suggest that the limbs should be rotated to the side (seamed edges contacting the ground) during crawling to maximize the stiffness and mitigate buckling at the limb-shoulder interface, regardless of the limb condition.

C. Hydrodynamic testing in flipper mode

We measured lift and drag forces on the limb (in flipper mode) in a laminar flow tank (Fig. 10a) using the same setup (1503 Gal recirculating system, 2.25 m × 0.45 m × 0.45 m) and method as in [13]. The angle of attack of the limb with respect to the incoming flow was adjusted. The lift and drag forces were acquired by a 6-axis Gamma DAQ F/T Transducer (ATI industrial), and a National Instruments DAQ (USB-6212) was used with a Matlab data acquisition toolbox to record force data.

Fig. 10b plots the glide ratio (F_L/F_D) with respect to the angle of attack (θ) at flow rates of 0.2-0.4 m/s. The hydrodynamic performance of the flipper in its jammed (stiff) and unjammed (soft) states are juxtaposed with those of the epoxy-based flippers from [13]. Desirable glide ratio

values, where lift forces experienced overcome drag forces, are highlighted green in the plots. Flow rates of 0.3 and 0.4 m/s result in similar performance patterns to the epoxy predecessor, with increased glide ratios occurring around 10°-15°. These desirable glide ratios were attained by the jamming flipper at each tested velocity. In contrast, the previous epoxy flipper was unable to reach glide ratios above 1 for speeds lower than 0.3 m/s. As the angle of attack increases, both flipper designs experience a decline in glide ratio characterized by mild fluctuations, ending in ratios around 1 at 25°.

IV. CONCLUSION

In this work, we proposed a refined morphing limb design intended for the next generation of the amphibious robotic turtle. The new morphing limb boasts temperature-agnostic morphing performance, addressing prior issues related to the use of thermally responsive materials, and drastically speeding up shape and stiffness transitions. Moreover, the new limb leverages a simplified morphing mechanism consisting of a single internal pouch actuator that applies positive pressure to the external layer jamming system. This positive pressure-reinforced jamming scheme reduces the number of layers needed to sustain a stable leg configuration under compressive loads. Thanks to the reduction in overall limb thickness due to positive pressure-reinforced jamming, the limb achieves favorable glide ratios at a wide range of flow velocities and angles of attack. Lastly, as a complement to the new morphing limb, we introduced a compact pneumatic control system. The improved morphing limb and its control module provide the foundation necessary to step toward the goal of an untethered, amphibious quadruped robot capable of autonomous multi-environment transitions.
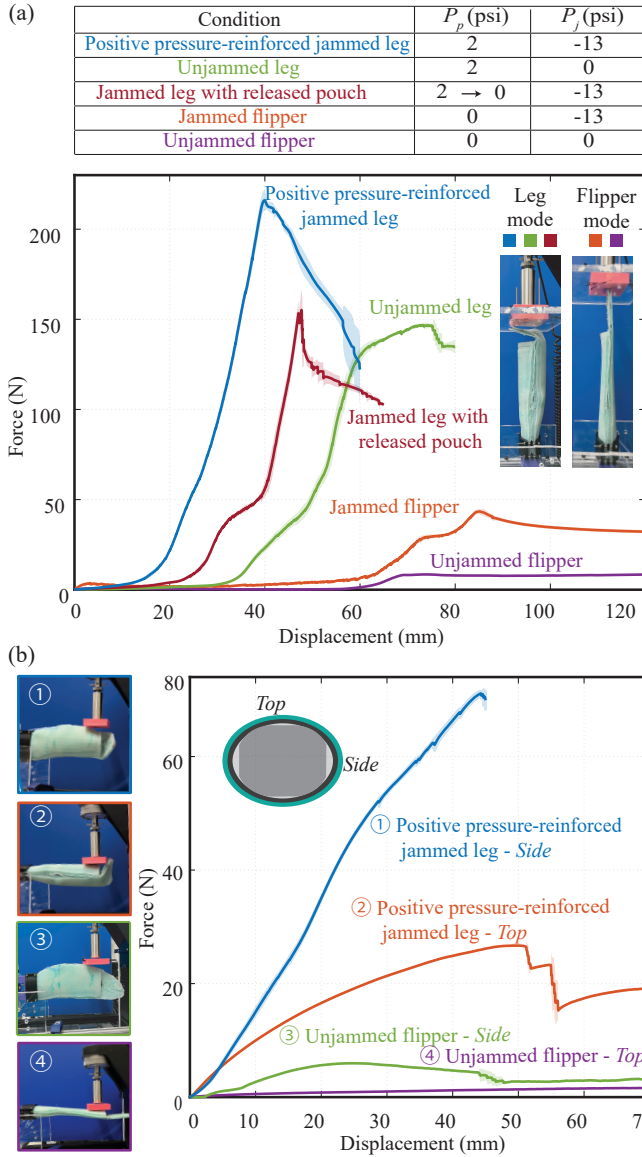
Fig. 9. (a) Vertical compression tests, representative of upright gaits, for five different limb inflation and stiffness conditions. (b) Horizontal loading tests, representative of crawling gaits, for two different limb conditions.
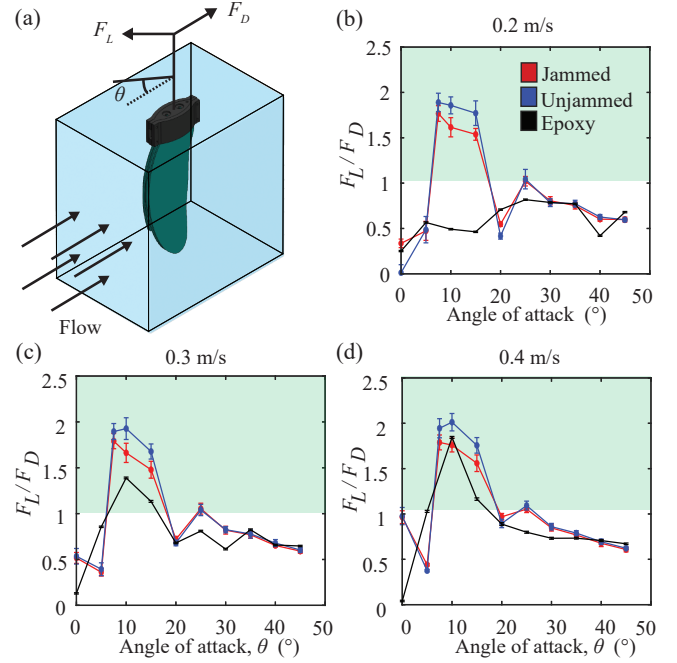

Fig. 10. (a) Setup for hydrodynamic testing. (b-d) Lift and drag force ratios for the morphing limb both jammed (stiff) and unjammed (soft), compared with the epoxy-based limb [13], respectively at 0.2, 0.3, and 0.4 m/s.

REFERENCES

[1] R. Baines, S. K. Patiballa, J. Booth, L. Ramirez, T. Sipple, A. Garcia, F. Fish, and R. Kramer-Bottiglio, "Multi-environment robotic transitions through adaptive morphogenesis," *Nature*, vol. 610, no. 7931, pp. 283–289, Oct. 2022.

[2] J. Sun, E. Lerner, B. Tighe, C. Middlemist, and J. Zhao, "Embedded shape morphing for morphologically adaptive robots," *Nature Communications*, vol. 14, no. 1, p. 6023, Sep. 2023.

[3] D. S. Shah, J. P. Powers, L. G. Tilton, S. Kriegman, J. Bongard, and R. Kramer-Bottiglio, "A soft robot that adapts to environments through shape change," *Nature Machine Intelligence*, vol. 3, no. 1, pp. 51–59, Jan. 2021.

[4] F. E. Fish, "Transitions from Drag-based to Lift-based Propulsion in Mammalian Swimming1," *American Zoologist*, vol. 36, no. 6, pp. 628–641, Dec. 1996.

[5] Q. Zhong, J. Zhu, F. E. Fish, S. J. Kerr, A. M. Downs, H. Bart-Smith, and D. B. Quinn, "Tunable stiffness enables fast and efficient swimming in fish-like robots," *Science Robotics*, vol. 6, no. 57, p. eabe4088, Aug. 2021.

[6] K. Caluwaerts, A. Iscen, J. C. Kew, W. Yu, T. Zhang, D. Freeman, K.-H. Lee, L. Lee, S. Saliceti, V. Zhuang *et al.*, "Barkour: Bench-marking animal-level agility with quadruped robots," *arXiv preprint arXiv:2305.14654*, 2023.

[7] X. Liang, M. Xu, L. Xu, P. Liu, X. Ren, Z. Kong, J. Yang, and S. Zhang, "The AmphiHex: A novel amphibious robot with transformable leg-flipper composite propulsion mechanism," in *2012 IEEE/RSJ International Conference on Intelligent Robots and Systems*, Oct. 2012, pp. 3667–3672.

[8] B. Zhong, S. Zhang, M. Xu, Y. Zhou, T. Fang, and W. Li, "On a CPG-Based Hexapod Robot: AmphiHex-II With Variable Stiffness Legs," *IEEE/ASME Transactions on Mechatronics*, vol. 23, no. 2, pp. 542–551, Apr. 2018.

[9] J. Sun and J. Zhao, "An Adaptive Walking Robot With Reconfigurable Mechanisms Using Shape Morphing Joints," *IEEE Robotics and Automation Letters*, vol. 4, no. 2, pp. 724–731, Apr. 2019.

[10] T. F. Nygaard, C. P. Martin, J. Torresen, K. Glette, and D. Howard, "Real-world embodied ai through a morphologically adaptive quadruped robot," *Nature Machine Intelligence*, vol. 3, no. 5, pp. 410–419, 2021.

[11] R. Gkliva and M. Kruusmaa, "Soft Fluidic Actuator for Locomotion in Multi-Phase Environments," *IEEE Robotics and Automation Letters*, vol. 7, no. 4, pp. 10 462–10 469, Oct. 2022.

[12] T. Kim, S. Lee, S. Chang, S. Hwang, and Y.-L. Park, "Environmental adaptability of legged robots with cutaneous inflation and sensation," *Advanced Intelligent Systems*, vol. 5, no. 11, p. 2300172, 2023.

[13] R. Baines, S. Freeman, F. Fish, and R. Kramer-Bottiglio, "Variable stiffness morphing limb for amphibious legged robots inspired by chelonian environmental adaptations," *Bioinspiration & Biomimetics*, vol. 15, no. 2, p. 025002, Feb. 2020.

[14] R. Baines, B. Yang, L. A. Ramirez, and R. Kramer-Bottiglio, "Kirigami layer jamming," *Extreme Mechanics Letters*, vol. 64, p. 102084, Nov. 2023.

[15] T. Liu, H. Xia, D.-Y. Lee, A. Firouzeh, Y.-L. Park, and K.-J. Cho, "A Positive Pressure Jamming Based Variable Stiffness Structure and its Application on Wearable Robots," *IEEE Robotics and Automation Letters*, vol. 6, no. 4, pp. 8078–8085, Oct. 2021.

[16] R. Niiyama, X. Sun, C. Sung, B. An, D. Rus, and S. Kim, "Pouch Motors: Printable Soft Actuators Integrated with Computational Design," *Soft Robotics*, vol. 2, no. 2, pp. 59–70, Jun. 2015.

[17] S. Wang, E. Frias Miranda, and L. H. Blumenschein, "The Folded Pneumatic Artificial Muscle (foldPAM): Towards Programmability and Control via End Geometry," *IEEE Robotics and Automation Letters*, vol. 8, no. 3, pp. 1383–1390, Mar. 2023.